Topological states and quantized current in helical organic molecules

Ai-Min Guo[1,*] and Qing-Feng Sun[2,3,†]
[1]*Department of Physics, Harbin Institute of Technology, Harbin 150001, China*
[2]*International Center for Quantum Materials, School of Physics, Peking University, Beijing 100871, China*
[3]*Collaborative Innovation Center of Quantum Matter, Beijing 100871, China*
(Received 24 March 2016; revised manuscript received 4 January 2017; published 10 April 2017)

We report a theoretical study of electron transport along helical organic molecules subject to an external electric field which is perpendicular to molecular helix axis. Our results reveal that topological states can appear in single-helical molecules as well as double-stranded DNA under the perpendicular electric field. In particular, a topological charge pumping can be realized by rotating the electric field in the transverse plane, where during each pumping cycle, an integer number of electrons can transport across the helical molecules at zero bias voltage, with pumped current being quantized. The quantized current constitutes multiple plateaus by scanning the Fermi energy as well as the bias voltage, and holds for various model parameters, since the edge states are topologically protected. These results could pave the way to explore topological states and quantized current in the biological systems and the helical molecules, and help in designing stable molecular devices.

DOI: 10.1103/PhysRevB.95.155411

I. INTRODUCTION

Helix structures are ubiquitous in both the biological world [1–3] and synthetic materials [4–6]. The electron transport along helical molecules, such as DNA and α-helical protein, has been receiving much attention among scientific communities [7–17], because this subject can enrich our knowledge regarding the electronic properties of low-dimensional systems due to unique helix structures and provide valuable information for understanding biological processes in living organisms [18–20]. It was reported by direct charge transport experiments that double-stranded DNA (dsDNA) could exhibit fascinating physical phenomena, such as the proximity-induced superconductivity [21], the negative differential resistance [22], and the piezoelectric effect [23]. Additionally, it was shown that both dsDNA and α-helical protein can behave as electric field-effect transistors [24–27] and as efficient spin filters [28–35].

On the other hand, topological insulators are very interesting systems that have an insulating gap in the bulk but usually possess robust conducting states on their edge or surface [36,37]. These conducting edge (surface) states are protected by specified symmetries and robust against disorders. Consequently, the topological quantum states have been attracting intense interest in condensed matter and materials physics. Recently, the topological states were found in two-dimensional (2D) organometallic frameworks [38–40], Su-Schrieffer-Heeger model [41–43], and one-dimensional inorganic systems, including photonic quasicrystals [44], optical lattices [45], atomic Bose-Einstein condensates [46,47], and double Peierls chain [48]. However, the topological states have not yet been reported in the biological systems or helical organic molecules.

In this paper, we first propose the topological states in single-helical molecules and the dsDNA under an external electric field which is perpendicular to molecular helix axis (z axis). Specially, a topological charge pumping occurs by rotating the electric field in the transverse plane (x-y plane). When the Fermi energy lies in bulk gaps, an integer number of electrons can transport across two-terminal systems at zero bias voltage and pumped current is quantized at $C \times e \times f$, with C being the sum of the Chern numbers of occupied energy bands, e the elementary charge, and f rotational frequency of the electric field. The quantized current forms several plateaus by sweeping either the Fermi energy or the bias voltage, and is very robust against perturbations. This is contrary to previous studies that the electron transport in the helical molecules strongly depends on external environments. This topological charge pumping may help in designing stable molecular devices and stimulate the role of topological phases in biological processes.

The rest of the paper is organized as follows. In Sec. II, we present a model Hamiltonian to describe electron transport along two-terminal helical molecules. In Secs. III and IV, we investigate the single-helical molecule and the dsDNA molecule, respectively. Then, the results are summarized in Sec. V. In Appendix A, we show the formula of current flowing through helical organic molecules. In Appendix B, the realization of a rotating electric field is provided. In Appendix C, we show the Chern number of both the single-helical molecule and the dsDNA molecule.

II. MODEL AND FORMULA

The electron transport through the two-terminal helical molecules can be simulated by the Hamiltonian: $\mathcal{H} = \mathcal{H}_m + \mathcal{H}_{el}$. Here, $\mathcal{H}_m$ is the molecular Hamiltonian as discussed later. $\mathcal{H}_{el} = \sum_{\beta,k}[\varepsilon_{\beta k} a^{\dagger}_{\beta k} a_{\beta k} + \sum_{j=1}^{J} t_{\beta}(a^{\dagger}_{\beta k} c_{jn_{\beta}} + \text{H.c.})]$ describes the left ($\beta = \text{L}$) and right ($\beta = \text{R}$) metal electrodes and their couplings to the molecule, with $n_{\text{L}} = 1$ and $n_{\text{R}} = N$. $a_{\beta k}/c_{jn_{\beta}}$ is the annihilation operator in the electrodes/molecule, J is the chain number, and N is the molecular length. The current flowing through helical organic molecules can be calculated by employing the Green's function. The detailed derivation of the current formula is attached in Appendix A.

*amguo@hit.edu.cn
†sunqf@pku.edu.cn

III. SINGLE-HELICAL MOLECULE

We first consider the simple case of $J = 1$, i.e., the single-helical molecules [49]. Then, the molecular Hamiltonian is [34,50,51]

$$\mathcal{H}_m^{(J=1)} = \sum_{n=1}^{N} \varepsilon_n c_n^\dagger c_n + \sum_{n=1}^{N-1} t c_n^\dagger c_{n+1} + \text{H.c.}, \tag{1}$$

where c_n annihilates an electron at site n with potential energy ε_n. The hopping integral t is set to the energy unit ($t = 1$ eV). In the presence of an external electric field E_g which is perpendicular to the helix axis, the potential energy takes the form [27,52]

$$\varepsilon_n = eV_g \cos(n\Delta\phi - \varphi). \tag{2}$$

Here, $2V_g = 2E_gR$ is the gate voltage drop across the helical molecules, R is the molecular radius, $\Delta\phi$ is the twist angle between neighboring sites, and the phase φ denotes the orientation of the electric field [52,53].

The molecular Hamiltonian in Eq. (1) is equivalent to the Harper-Hofstadter model which is projected from a 2D square lattice in the presence of uniform magnetic field [54,55], with $\alpha = \Delta\phi/2\pi$ mapping to magnetic flux per primitive cell. Then, it can be seen from Fig. 1(a) that for the single-helical molecule, two edge states traverse each bulk gap and intersect at specific values of φ [56]. Figures 2(a)–2(d) present spatial distribution of electron density p_n for four edge states of the single-helical molecule, where the edge states are on the red dashed-dot line in Fig. 1(a). Here, $p_n = |\psi_n|^2$ and ψ_n is the amplitude of the wave function of a specific edge state at site n of the helical molecule. It clearly appears that the edge states are localized in either the left end or the right end of the helical molecule. These edge states are topologically protected against perturbations, just as those in 2D quantum Hall systems [57]. These topological edge states can be characterized by the Chern number (the method to calculate the Chern number and the corresponding Chern number of the helical molecules are shown in Appendix C), which is calculated on a discretized Brillouin zone [58] and is the $\mathbb{Z}$ topological invariant [59,60]. Since the edge states are localized in either end of the molecule, the electron densities p_1 and p_N at the end sites are quite large, as illustrated in Fig. 1(c). Both p_1 and p_N are independent of the molecular length N, implying that the edge states should be robust against perturbations such as the molecular length. In contrast, the bulk states always locate in the energy band. Because of the spatially extended wave function, both p_1 and p_N are quite small and decrease with increasing N as $p_n \propto N^{-1}$ [see Fig. 1(b)].

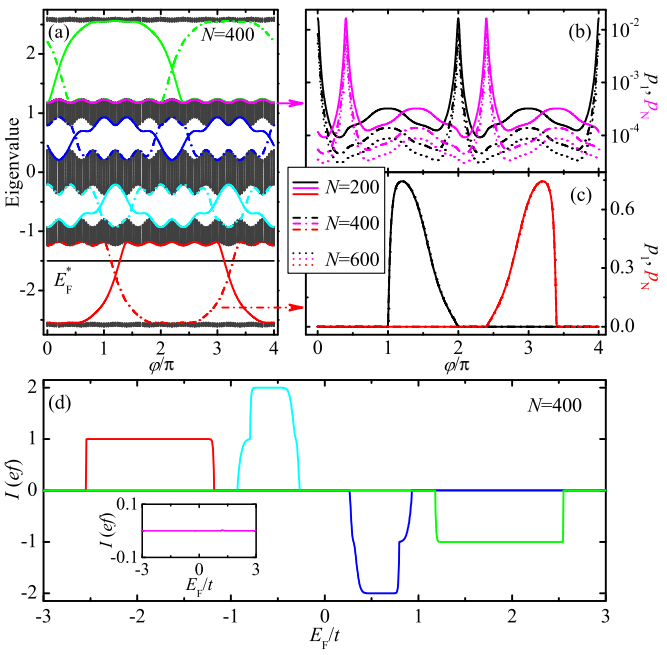

FIG. 1. (a) Energy spectrum of the single-helical molecule under open boundary conditions. The colored lines across the energy gaps are the topological edge states. Phase-dependent electron densities p_1 and p_N at the end sites of the single-helical molecule for (b) a typical bulk state and for (c) an edge state with various molecular lengths N, as depicted by the arrows. (d) Pumped current I vs Fermi energy E_F for all the topological edge states, where each line corresponds to the edge states with the same color in (a). The inset shows I for the bulk state which is indicated by the magenta line in (a). The parameters are $\alpha = 1/5$ and $V_g = 1.5$.

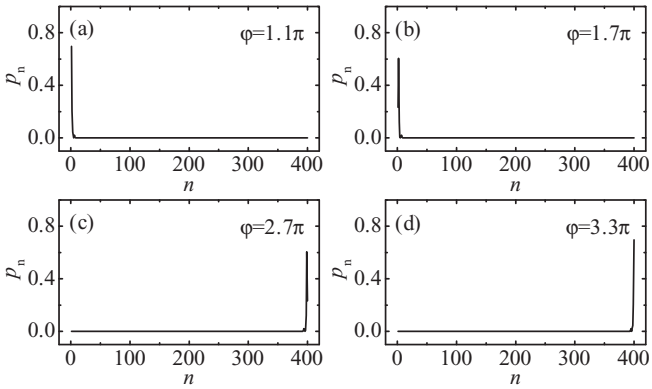

FIG. 2. Spatial distribution of electron density p_n for typical edge states on the red dashed-dot line in Fig. 1(a). The edge states locate in the bottom bulk gap, and the phase is (a) $\varphi = 1.1\pi$, (b) $\varphi = 1.7\pi$, (c) $\varphi = 2.7\pi$, and (d) $\varphi = 3.3\pi$.

The topological edge states can dramatically affect the charge transport properties of the helical molecule and we consider a two-terminal setup. Figure 1(d) shows pumped current I, the current at zero bias voltage, for the single-helical molecule during one pumping cycle. Here, the phase $\varphi = 2\pi f\tau$ is varied from 0 to 2π by rotating the electric field in the transverse plane, $f = 10^6$ Hz is the rotational frequency, and τ is the time (see Appendix B for the realization of a rotating electric field). It clearly appears that the pumped current is quantized at integer multiples of ef and constitutes plateaus by scanning E_F, implying that the singe-helical molecule transfers an integer number of electrons (holes) for $E_F < 0$ ($E_F > 0$). The number of transmitted charges in each cycle equals that of intersection points between the edge states, i.e., the sum of the Chern numbers of the occupied energy bands (see Appendix C). We consider the edge state, indicated by the red dashed-dot line in Fig. 1(a), as an example and elucidate the underlying physics of this adiabatic charge pumping. The Fermi energy $E_F^\star$ lies in the bottom bulk gap, as shown by the black solid line in Fig. 1(a). At $\varphi = 0$ ($\tau = 0$), the edge

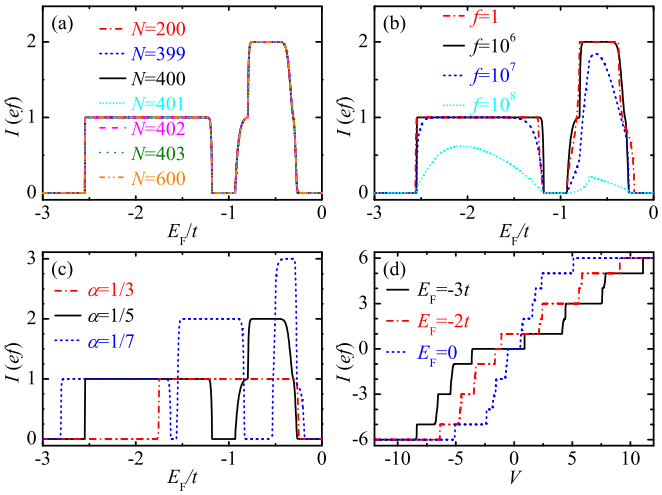

FIG. 3. Pumped current I of the single-helical molecule with (a) different molecular lengths N, (b) various rotational frequencies f, and (c) several twist angles $\Delta\phi = 2\pi\alpha$, where the black solid lines are shown for reference with $\alpha = 1/5$, $V_g = 1.5$, $N = 400$, and $f = 10^6$ Hz. (d) Current I vs bias voltage V for three E_F.

state locates above $E_F^\star$ and is empty. For a critical φ (τ) when the state passes through the Fermi level, an electron will be injected into the edge state from the left electrode and localized in the left end of the molecule. Then, the edge state is occupied. By further increasing φ (τ), the electron in the state transports from the left end to the right one [see Fig. 1(c)]. When the energy of the state surpasses $E_F^\star$, the electron is transmitted from the edge state to the right electrode and the state becomes empty again. As a result, an electron is pumped across the molecule per two pumping cycles and similar phenomena can be observed regarding the other topological edge states. It is now clear that this adiabatic charge pumping is driven by the topological nature of the edge states and thus topologically protected against perturbations unless the energy gap closes up. While for the bulk state, the pumped current is negligible with the order of magnitude being 10^{-3} [see the inset of Fig. 1(d)]. In what follows, we focus on the topological edge states, since the bulk states are fragile upon perturbations and their energy range differs from the topological edge states.

To verify the robustness of the topological charge pumping, Figs. 3(a)–3(c) plot the pumped current I under a variety of situations. One notices that the I-E_F curves are identical to each other for different molecular lengths [see Fig. 3(a)]. The plateaus of quantized currents persist in a very broad range of the frequencies, from $f = 1$ to 10^7 Hz [see $I = ef$ in Fig. 3(b)]. However, by further increasing f, the pumped current will be declined over the entire energy spectrum and all the plateaus are destroyed, because the speed of electron tunneling between the molecule and the electrodes cannot keep up with the rotation rate of the electric field. Besides, the topological charge pumping still holds for different single-helical molecules with various twist angles. The number of plateaus increases with decreasing α and the width becomes narrower when the current is larger [see Fig. 3(c)], since the number and the width of the bulk gaps are changed.

The plateaus of quantized currents can also be maintained at relatively high temperatures and in a very wide region of the

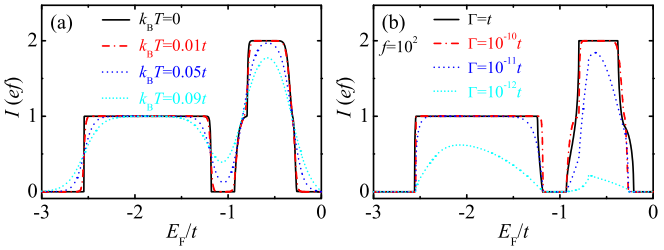

FIG. 4. Pumped current I of the single-helical molecule with (a) different temperatures T and (b) various coupling strengths Γ between the molecule and the electrodes. Here, k_B is the Boltzmann constant, and the other parameters are $\alpha = 1/5$, $V_g = 1.5$, $N = 400$, $f = 10^6$ Hz, $\Gamma = 10^{-6}t$, and $T = 0$, unless stated in the figure.

coupling between the molecule and the electrodes. Figure 4(a) shows the pumped current I versus the Fermi energy E_F for the single-helical molecule with different temperatures T. It can be seen that both plateaus of quantized currents can be maintained at nonzero temperatures [see the red dashed-dot line in Fig. 4(a)] and the lower one persists with the temperature up to $k_B T = 0.09t$ [see the cyan dotted line in Fig. 4(a)]. The wider the bulk gap is, the higher temperature the plateaus of quantized currents can persist. Figure 4(b) displays I versus E_F by considering various coupling strengths between the molecule and the electrodes, with $f = 10^2$ Hz. The lower plateau of quantized current can hold by changing Γ from t to $10^{-11}t$. However, by further decreasing Γ, the pumped current will be decreased over the whole energy spectrum and all the plateaus are destroyed, because the speed of electron tunneling between the molecule and the electrodes is too slow.

When the bias voltage V is applied between the left and right electrodes, the current is also quantized at integer multiples of ef and forms several plateaus in the I-V curves [see Fig. 3(d)]. The I-V curve is centrally symmetric for $E_F = 0$ due to the central symmetry of the I-E_F curve [see Fig. 1(d)], and is asymmetric for $E_F \neq 0$. Therefore, we conclude that the topological charge pumping is robust, and the plateaus of quantized currents can be observed in the I-E_F curve at zero bias voltage and in the I-V curve within a wide range of model parameters.

IV. DOUBLE-STRANDED DNA MOLECULE

We then study the topological charge pumping in the dsDNA molecule under the electric field E_g [see Fig. 5(a)]. The Hamiltonian of the dsDNA molecule is [26,30,51]

$$\mathcal{H}_m^{(J=2)} = \sum_{j=1}^{2}\sum_{n=1}^{N} \varepsilon_{jn} c_{jn}^\dagger c_{jn} + \sum_{j=1}^{2}\sum_{n=1}^{N-1} t c_{jn}^\dagger c_{jn+1} + \sum_{n=1}^{N} \lambda c_{1n}^\dagger c_{2n} + \text{H.c.}, \quad (3)$$

which can be regarded as coupling two single-helical molecules. Here, c_{jn} annihilates an electron at site n of chain j and each lattice site denotes one nucleobase [see Fig. 5(a)]. The potential energy is [26,27,53]

$$\varepsilon_{jn} = -(-1)^j [eV_g \cos(n\Delta\phi - \varphi) + \Delta\varepsilon], \quad (4)$$

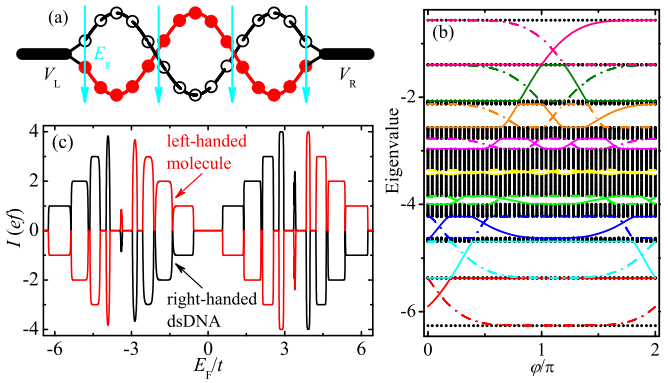

FIG. 5. (a) Sketch of a two-terminal dsDNA under a perpendicular electric field E_g, where the full and open circles represent the nucleobases. (b) Energy spectrum of the dsDNA under open boundary conditions. Because of the particle-hole symmetry, the energy spectrum is symmetric with respect to the line $E = 0$ and not shown above $E = 0$. (c) Pumped current I vs E_F for the right-handed dsDNA and the left-handed molecule at zero bias voltage. The parameters are $V_g = 1.5$, $N = 200$, $f = 10^6$ Hz, $\Delta\varepsilon = 3t$, and $\lambda = 1.5t$.

where $\Delta\phi = 2\pi/10$ is the twist angle between neighboring base pairs, $2\Delta\varepsilon$ is the potential energy difference between the two chains of a homogeneous dsDNA at $V_g = 0$, and the other parameters are the same as Eq. (2). Here, the interchain hopping integral is $\lambda = 1.5t$ and the potential energy is chosen as $\Delta\varepsilon = 3t$, which are extracted from the experimental results [61] and first-principles calculations [62–64].

One can see from Fig. 5(b) that the lower energy spectrum ($E < 0$) of the dsDNA consists of ten subbands as expected. A pair of edge states traverse each energy gap and intersect at specific values of φ. Identical features can be found in the upper energy spectrum ($E > 0$), due to the particle-hole symmetry. Consequently, the topological charge pumping can also be observed in the dsDNA that the pumped current is quantized at integer multiples of ef and forms plateaus by scanning E_F, as indicated by the black line in Fig. 5(c). The plateaus locate at the energy gaps and will not be affected by the bulk states. When the plateau is farther away from the lower (upper) band center, it is wider and more robust because of larger energy gap [see Fig. 5(b)]. Besides, the pumped current presents alternating electronlike behavior ($I > 0$) and holelike behavior ($I < 0$) in the energy spectrum. When the chirality of the molecule is changed from the right-handed species to the left-handed one by using the reflection operation, the direction of the current is reversed [see Fig. 5(c)], i.e., $I(\Delta\phi) = -I(-\Delta\phi)$.

Figure 6 displays the pumped current of the dsDNA under various model parameters. For $V_g = 0$, all the electronic states are trivial and the pumped current is zero [see the cyan dotted line in Fig. 6(a)]. When the gate voltage is implemented, the topological edge states emerge and give rise to plateaus of quantized currents, even for small gate voltage of $V_g = 0.2$ [see the blue dashed line in Fig. 6(a)]. By increasing V_g, the original plateaus broaden and new ones of large I gradually appear. As $\Delta\varepsilon$ rises, the I-E_F curve is translated toward lower energy and the plateaus keep almost unchanged [see Fig. 6(b)]. Additionally, the plateaus of quantized currents can occur in a very wide

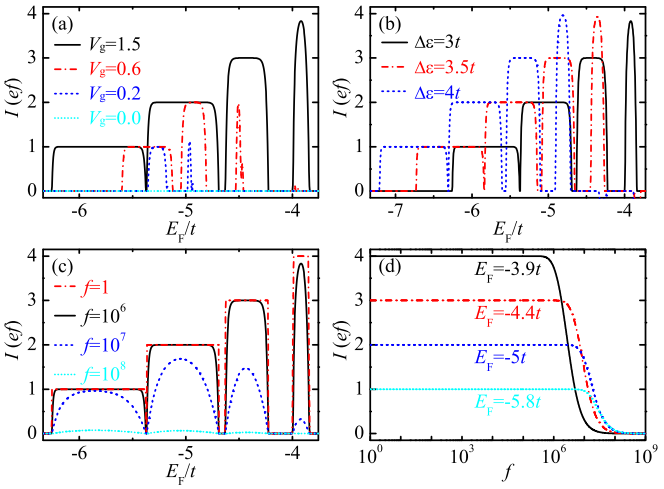

FIG. 6. Pumped current I of the dsDNA with (a) several V_g, (b) three $\Delta\varepsilon$, and (c) different f, where the other parameters are the same as Fig. 5(c). (d) I vs f for the dsDNA with several E_F.

range of f [see Fig. 6(c)] and those of smaller I are more robust against a faster rotation of the electric field [see Fig. 6(d)].

Figures 7(a) and 7(b) show I versus E_F for the dsDNA molecule by considering different temperatures T and various coupling strengths Γ between the molecule and the electrodes, respectively. Similar phenomena can also be found for the dsDNA molecule that the plateaus of quantized currents can persist at nonzero temperatures and the lowest one remains with the temperature up to $k_B T = 0.09t$ [see Fig. 7(a)]. When $t = 0.1$ eV, the temperature T is about 100 K for $k_B T = 0.09t$. Notice that the hopping integral of the dsDNA molecule can be larger than 0.1 eV, as demonstrated by first-principles calculations [62,63]. Consequently, the plateaus of quantized currents can be observed at relatively high temperatures. In addition, these plateaus can also persist in a very broad range of Γ, from $\Gamma = t$ to $10^{-10}t$ [see Fig. 7(b)]. Therefore, we conclude that the topological charge pumping of the dsDNA arises from its intrinsic helix structure, and the quantized current is very robust and could be detected in the experiments.

Finally, we study the current of the dsDNA at nonzero bias voltages, as shown in Fig. 8. Because of the topological charge pumping, the plateaus of quantized currents emerge at integer multiples of ef for both the dsDNA and the left-handed molecule, where both I-V curves are asymmetric [see

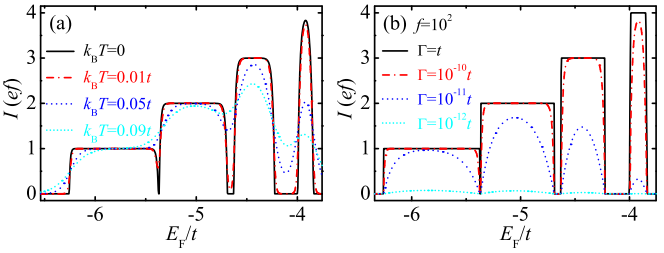

FIG. 7. Pumped current I of the dsDNA molecule with (a) a variety of temperatures T and (b) different coupling strengths Γ between the molecule and the electrodes. The parameters are $V_g = 1.5$, $N = 200$, $f = 10^6$ Hz, $\Delta\varepsilon = 3t$, $\lambda = 1.5t$, $\Gamma = 10^{-6}t$, and $T = 0$, unless presented in the figure.

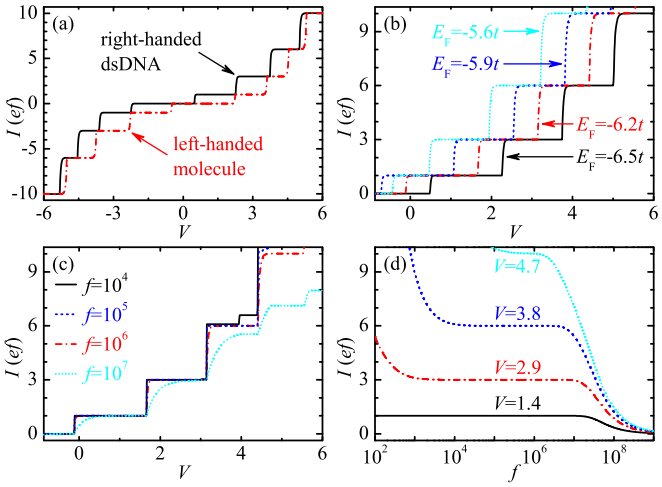

FIG. 8. I-V curves for (a) the dsDNA and the left-handed molecule with $E_F = -6.5t$, for the dsDNA with (b) several E_F and (c) various f by fixing $E_F = -6.2t$. (d) I vs f for the dsDNA with $E_F = -6.2t$. The other parameters are the same as Fig. 5(c).

Fig. 8(a)]. For instance, the current of the dsDNA is $I = ef$ for $V \in (0.6, 2.1)$ and vanishes for $V \in (-2.1, -0.6)$, implying that the dsDNA can serve as a molecular switch by reversing the bias voltage. When the Fermi energy is increased, the I-V curve is shifted toward lower bias voltage and the plateaus remain almost the same [see Fig. 8(b)]. It is interesting that the current can also flow through the molecule from the left electrode to the right one even if the chemical potential of the right electrode is higher ($\mu_R > \mu_L$), i.e., I is positive at $V < 0$ [see Figs. 8(b) and 3(d)]. This arises from the fact that the direction of I keeps the same when μ_L and μ_R locate in the same energy gap, which is induced by the topological charge pumping. Similarly, the plateaus of the I-V curve can exist in a rather broad range of f [see Fig. 8(c)] and those of smaller I are more robust [see Fig. 8(d)]. Therefore, the plateaus of quantized currents also appear in the I-V curve of the dsDNA at nonzero bias voltages.

V. CONCLUSIONS

We show that topological states could emerge in helical organic molecules, such as single-helical molecules and double-stranded DNA, in the presence of a perpendicular electric field. A topological charge pumping is predicted by rotating the electric field in the transverse plane and an integer number C of electrons can be transmitted through the helical molecules in each pumping cycle, with C being the sum of the Chern numbers of the occupied energy bands. Additionally, the quantized current forms multiple plateaus by scanning the Fermi energy or the bias voltage. These plateaus are very robust and of measurable width, and may thus be realized in the charge transport experiments.

ACKNOWLEDGMENTS

This work was supported by National Basic Research Program of China (Grant No. 2015CB921102), National Natural Science Foundation of China under Grants No. 11274364, No. 11504066, and No. 11574007, and Fundamental Research Funds for the Central Universities of China under Grant No. AUGA5710013615. We thank Q. Zhu, T.-F. Fang, and H. Liu for helpful discussions.

APPENDIX A: FORMULA OF CURRENT FLOWING THROUGH HELICAL ORGANIC MOLECULES

The current of an energy level can be calculated by employing the Green's function and we take the single-helical molecule as an example. The Hamiltonian of the single-helical molecule is [34,50,51]

$$\mathcal{H}_m^{(J=1)} = \sum_{n=1}^{N} \varepsilon_n c_n^\dagger c_n + \sum_{n=1}^{N-1} t c_n^\dagger c_{n+1} + \text{H.c.} \tag{A1}$$

By diagonalizing its matrix form, the molecular Hamiltonian in Eq. (A1) can be rewritten as

$$\mathcal{H}_m^{(J=1)} = \sum_{j=1}^{N} E_j b_j^\dagger b_j. \tag{A2}$$

Here, E_j is the eigenvalue of the jth eigenstate, $b_j^\dagger = \sum_{n=1}^{N} c_n^\dagger \psi_{nj}$, and ψ_{nj} is the amplitude of the wave function of the jth eigenstate at site n of the molecule. Then, the Hamiltonians of the two electrodes and their couplings to the molecule are expressed as

$$\mathcal{H}_{el} = \sum_{\beta,k} \left[\varepsilon_{\beta k} a_{\beta k}^\dagger a_{\beta k} + \sum_{j=1}^{N} t_\beta (\psi_{n_\beta j} a_{\beta k}^\dagger b_j + \text{H.c.}) \right], \tag{A3}$$

where $\beta = \text{L/R}$ stands for the left/right electrode, $n_L = 1$, and $n_R = N$. When the gate electric field rotates in the transverse plane, the electronic structure of the molecule will be modified. This is attributed to the fact that the phase $\varphi = 2\pi f \tau$ varies as the time τ evolves and the on-site energy ε_n is changed, with $f = \omega/2\pi$ the rotational frequency. Provided that the electron occupation number is n_j in the jth energy level, we have

$$\frac{dn_j}{d\tau} = \frac{1}{i\hbar} \langle [b_j^\dagger b_j, \mathcal{H}] \rangle. \tag{A4}$$

After some algebra calculations, the occupation number takes the form

$$\frac{dn_j}{d\tau} = \frac{1}{\hbar} [\tilde{\Gamma}_L f_L + \tilde{\Gamma}_R f_R] - \frac{1}{\hbar} (\tilde{\Gamma}_L + \tilde{\Gamma}_R) n_j, \tag{A5}$$

where $\hbar$ is the reduced Planck constant, $\tilde{\Gamma}_L = \Gamma_L |\psi_{1j}|^2 = \Gamma_L p_{1j}$, $\tilde{\Gamma}_R = \Gamma_R |\psi_{Nj}|^2 = \Gamma_R p_{Nj}$, and $f_{L/R} = \{1 + \exp[(E - \mu_{L/R})/k_B T]\}^{-1}$ is the Fermi-Dirac distribution function. Here, $\Gamma_{L/R} = 2\pi\rho |t_{L/R}|^2$ is the coupling strength between the molecule and the left/right electrode, $p_{1j/Nj}$ is the electron density of the jth eigenstate at the end site $1/N$ of the molecule, and ρ is the density of states of the electrode. $\mu_{L/R}$ is the chemical potential of the left/right electrode, k_B is the Boltzmann constant, and T is the temperature. The occupation number can be obtained by solving Eq. (A5) self-consistently. Then, in time interval $\Delta\tau$, the electrons flowing through the

electrode β can be expressed as

$$\Delta n_{\beta j} = \frac{1}{\hbar}\tilde{\Gamma}_\beta f_\beta \Delta\tau + \frac{\tilde{\Gamma}_\beta}{\tilde{\Gamma}_L + \tilde{\Gamma}_R}[n_j(\tau+\Delta\tau) - n_j(\tau) - \frac{\Delta\tau}{\hbar}(\tilde{\Gamma}_L f_L + \tilde{\Gamma}_R f_R)]. \quad \text{(A6)}$$

Finally, during one pumping cycle where the phase φ is changed from zero to 2π, the electrons $\langle n_{\beta j}\rangle$ transmitted through the molecule are the sum over all the time intervals and the current is

$$I = ef\sum_{j=1}^{N}\langle n_{Lj}\rangle. \quad \text{(A7)}$$

In this paper, the coupling strengths between the molecule and the electrodes are set to $\Gamma_L = \Gamma_R = \Gamma = 10^{-6}t$ unless otherwise noted, with t the hopping integral. And our results still hold when other values of Γ are considered.

APPENDIX B: REALIZATION OF A ROTATING ELECTRIC FIELD

The rotating electric field can be realized by using three gate electrodes with alternating voltages, as discussed below. Figure 9 presents the projections of a helical organic molecule (black circle in the center) and three gate electrodes (three rectangles with different colors) in the transverse plane (x-y plane). In the presence of these gate electrodes with voltages V_{gj}, three electric fields $\vec{E}_{gj}$ emerge spontaneously, with $j = 1$, 2, and 3. When the voltages V_{gj} are alternating ones, the magnitude of the electric fields can take the form

$$E_{gj} = (2E_g/3)\cos[\omega\tau - 2\pi(j-1)/3]. \quad \text{(B1)}$$

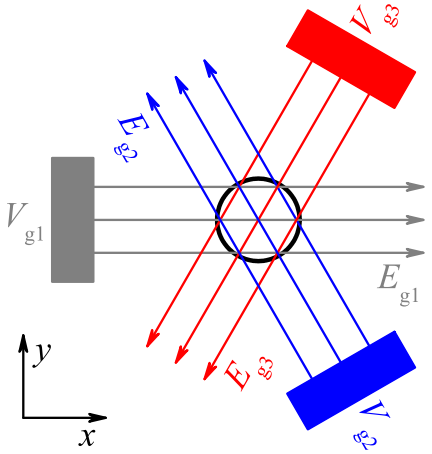

FIG. 9. Schematic view of a helical organic molecule and three gate electrodes along the helix axis (z axis), where the black circle in the center and the three rectangles are, respectively, the projections of the helical organic molecule and the gate electrodes in the x-y plane. An electric field $\vec{E}_{gj}$ emerges spontaneously under each gate electrode with voltage V_{gj}, where $j = 1, 2$, and 3. The direction of the gate electric fields is depicted by the arrows, as further illustrated in the following. $\vec{E}_{g1}$ is parallel to the x axis, and the angle between $\vec{E}_{g2}$ ($\vec{E}_{g3}$) and the x axis is $2\pi/3$ ($4\pi/3$). In the presence of the alternating voltages V_{gj}, the total electric field $\vec{E}_g = \sum_{j=1}^{3}\vec{E}_{gj}$ could rotate in the x-y plane.

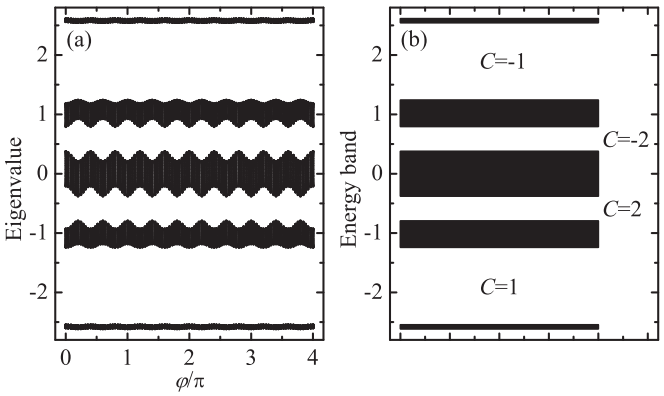

FIG. 10. (a) Energy spectrum of the single-helical molecule with periodic boundary conditions. (b) The corresponding energy bands and the Chern number C when all the energy bands are fully filled below a specific bulk gap. Here, the parameters are the same as Fig. 1(a) in the main text. One can see that all the topological edge states vanish under the periodic boundary conditions.

Here, $2E_g/3$ is the amplitude, ω is the angular frequency, and τ is the time. The last term is the phase which is different for various electric fields. The direction of the electric fields is described by the arrows in Fig. 9 and further demonstrated in the caption. Then, the total electric field traversing the helical organic molecule is $\vec{E}_g = \sum_{j=1}^{3}\vec{E}_{gj}$. By performing simple analytical calculations, the x and y components of $\vec{E}_g$ are expressed as $E_{gx} = E_g\cos(\omega\tau)$ and $E_{gy} = E_g\sin(\omega\tau)$, respectively. $\vec{E}_g$ is just the rotating electric field, whose strength E_g is constant and direction rotates in the transverse plane as the time τ evolves. Since the electric field can travel through vacuum and dielectric materials, the three gate electrodes in Fig. 9 can be far away from the helical molecules.

In the presence of the rotating electric field $\vec{E}_g$, the potential energy of the single-helical molecule is

$$\varepsilon_n = eE_gR\cos(n\Delta\phi - \omega\tau), \quad \text{(B2)}$$

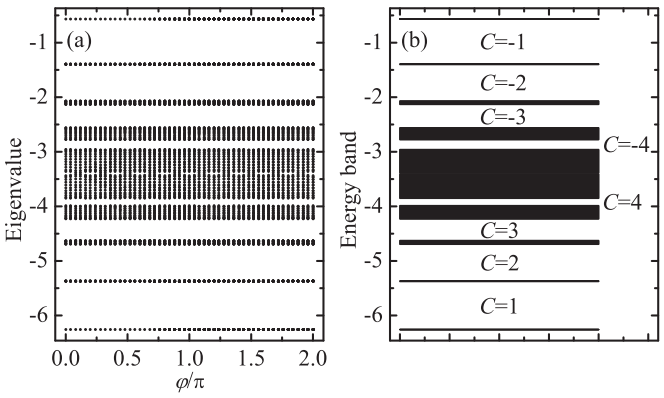

FIG. 11. (a) Energy spectrum of the dsDNA molecule with periodic boundary conditions. The energy spectrum is not displayed for $E > 0$, because of the particle-hole symmetry. (b) The corresponding energy bands and the Chern number C when all the energy bands are completely occupied below a specific bulk gap. Here, the parameters are the same as Fig. 5(b) in the main text. All the topological edge states also disappear in the energy spectrum of the dsDNA molecule with the periodic boundary conditions.

which is exactly Eq. (2) in the main text and $\omega\tau = \varphi$. Therefore, the rotating electric field can be realized by using several gate electrodes with alternating voltages.

APPENDIX C: CHERN NUMBER OF HELICAL ORGANIC MOLECULES

Next, we explore the topological properties of the helical organic molecules with periodic boundary conditions and calculate the Chern number. It is expected that in the presence of the periodic boundary conditions, all the topological edge states disappear for both the single-helical molecule and the double-stranded DNA (dsDNA) molecule, as illustrated in Figs. 10(a) and 11(a), respectively. In this situation, the momentum k becomes a good quantum number and the Hamiltonian can be expressed in the k space, because of the translational symmetry. For instance, the Hamiltonian in the k space for the single-helical molecule with $\alpha = 1/5$ takes the form

$$\mathcal{H}_k^{(J=1)} = \begin{pmatrix} \varepsilon_1 & t & 0 & 0 & te^{-5ik} \\ t & \varepsilon_2 & t & 0 & 0 \\ 0 & t & \varepsilon_3 & t & 0 \\ 0 & 0 & t & \varepsilon_4 & t \\ te^{5ik} & 0 & 0 & t & \varepsilon_5 \end{pmatrix}. \tag{C1}$$

It is obvious that there exist five energy bands for the Hamiltonian in Eq. (C1), as further demonstrated in Figs. 10(a) and 10(b). When the gate electric field $\vec{E}_g$ rotates in the transverse plane, the phase φ will be changed and a series of Hamiltonians $\mathcal{H}_{k,\varphi}$ can be derived in the k-φ space. By diagonalizing $\mathcal{H}_{k,\varphi}$, we obtain normalized wave functions $\psi_n(k,\varphi)$ of the nth energy band and the corresponding Chern number is calculated by

$$C_n = \frac{1}{2\pi i}\int_0^{2\pi} d\varphi \int_0^{2\pi\alpha} dk \left[\left\langle \frac{\partial\psi_n(k,\varphi)}{\partial\varphi}\middle|\frac{\partial\psi_n(k,\varphi)}{\partial k}\right\rangle - \left\langle \frac{\partial\psi_n(k,\varphi)}{\partial k}\middle|\frac{\partial\psi_n(k,\varphi)}{\partial\varphi}\right\rangle\right]. \tag{C2}$$

Here, we employ the method in Ref. [58] to calculate the Chern number, which is performed on a discretized Brillouin zone. Finally, for a specific Fermi energy which locates in the bulk gap, the rescaled Chern number C is defined as the sum of the Chern number C_n of all the occupied energy bands. Figures 10(b) and 11(b) present the Chern number C of the single-helical molecule and the dsDNA molecule, respectively. It can be seen that for a certain Fermi energy which lies in the bulk gap, the Chern number C is equal to the quantized current I in units of ef. This implies that the quantized current is topologically protected and robust against perturbations until the closure of the bulk gap.

[1] N. C. Seeman, Nature (London) **421**, 427 (2003).
[2] R. G. Endres, D. L. Cox, and R. R. P. Singh, Rev. Mod. Phys. **76**, 195 (2004).
[3] J. C. Genereux and J. K. Barton, Chem. Rev. **110**, 1642 (2010).
[4] T. Nakano and Y. Okamoto, Chem. Rev. **101**, 4013 (2001).
[5] P. X. Gao, Y. Ding, W. Mai, W. L. Hughes, C. Lao, and Z. L. Wang, Science **309**, 1700 (2005).
[6] E. Yashima, K. Maeda, H. Iida, Y. Furusho, and K. Nagai, Chem. Rev. **109**, 6102 (2009).
[7] H. Cohen, C. Nogues, R. Naaman, and D. Porath, Proc. Natl. Acad. Sci. USA **102**, 11589 (2005).
[8] X. Guo, A. A. Gorodetsky, J. Hone, J. K. Barton, and C. Nuckolls, Nat. Nanotechnol. **3**, 163 (2008).
[9] J. D. Slinker, N. B. Muren, S. E. Renfrew, and J. K. Barton, Nat. Chem. **3**, 228 (2011).
[10] Y. A. Berlin, A. A. Voityuk, and M. A. Ratner, ACS Nano **6**, 8216 (2012).
[11] N. Renaud, Y. A. Berlin, F. D. Lewis, and M. A. Ratner, J. Am. Chem. Soc. **135**, 3953 (2013).
[12] L. Xiang, J. L. Palma, C. Bruot, V. Mujica, M. A. Ratner, and N. Tao, Nat. Chem. **7**, 221 (2015).
[13] Y. Jin, N. Friedman, M. Sheves, T. He, and D. Cahen, Proc. Natl. Acad. Sci. USA **103**, 8601 (2006).
[14] T. R. Prytkova, I. V. Kurnikov, and D. N. Beratan, Science **315**, 622 (2007).
[15] A. N. Aleshin, H. J. Lee, Y. W. Park, and K. Akagi, Phys. Rev. Lett. **93**, 196601 (2004).
[16] S. S. Skourtis, D. N. Beratan, R. Naaman, A. Nitzan, and D. H. Waldeck, Phys. Rev. Lett. **101**, 238103 (2008).
[17] P. C. Mondal, N. Kantor-Uriel, S. P. Mathew, F. Tassinari, C. Fontanesi, and R. Naaman, Adv. Mater. **27**, 1924 (2015).
[18] S. M. Gasper and G. B. Schuster, J. Am. Chem. Soc. **119**, 12762 (1997).
[19] E. Meggers, D. Kusch, M. Spichty, U. Wille, and B. Giese, Angew. Chem. Int. Ed. **37**, 460 (1998).
[20] E. Yavin, A. K. Boal, E. D. A. Stemp, E. M. Boon, A. L. Livingston, V. L. O'Shea, S. S. David, and J. K. Barton, Proc. Natl. Acad. Sci. USA **102**, 3546 (2005).
[21] A. Y. Kasumov, M. Kociak, S. Guéron, B. Reulet, V. T. Volkov, D. V. Klinov, and H. Bouchiat, Science **291**, 280 (2001).
[22] P.-C. Jangjian, T.-F. Liu, M.-Y. Li, M.-S. Tsai, and C.-C. Chang, Appl. Phys. Lett. **94**, 043105 (2009).
[23] C. Bruot, J. L. Palma, L. Xiang, V. Mujica, M. A. Ratner, and N. Tao, Nat. Commun. **6**, 8032 (2015).
[24] K.-H. Yoo, D. H. Ha, J.-O. Lee, J. W. Park, J. Kim, J. J. Kim, H.-Y. Lee, T. Kawai, and H. Y. Choi, Phys. Rev. Lett. **87**, 198102 (2001).
[25] G. Maruccio, A. Biasco, P. Visconti, A. Bramanti, P. P. Pompa, F. Calabi, R. Cingolani, R. Rinaldi, S. Corni, R. Di Felice, E. Molinari, M. P. Verbeet, and G. W. Canters, Adv. Mater. **17**, 816 (2005).
[26] A. V. Malyshev, Phys. Rev. Lett. **98**, 096801 (2007).
[27] S. Roy, H. Vedala, A. D. Roy, D.-H. Kim, M. Doud, K. Mathee, H.-K. Shin, N. Shimamoto, V. Prasad, and W. Choi, Nano Lett. **8**, 26 (2008).
[28] S. Yeganeh, M. A. Ratner, E. Medina, and V. Mujica, J. Chem. Phys. **131**, 014707 (2009).

[29] B. Göhler, V. Hamelbeck, T. Z. Markus, M. Kettner, G. F. Hanne, Z. Vager, R. Naaman, and H. Zacharias, Science **331**, 894 (2011).
[30] A.-M. Guo and Q.-F. Sun, Phys. Rev. Lett. **108**, 218102 (2012).
[31] R. Gutierrez, E. Díaz, R. Naaman, and G. Cuniberti, Phys. Rev. B **85**, 081404(R) (2012).
[32] E. Medina, F. López, M. A. Ratner, and V. Mujica, Europhys. Lett. **99**, 17006 (2012).
[33] D. Mishra, T. Z. Markus, R. Naaman, M. Kettner, B. Göhler, H. Zacharias, N. Friedman, M. Sheves, and C. Fontanesi, Proc. Natl. Acad. Sci. USA **110**, 14872 (2013).
[34] A.-M. Guo and Q.-F. Sun, Proc. Natl. Acad. Sci. USA **111**, 11658 (2014).
[35] E. Medina, L. A. González-Arraga, D. Finkelstein-Shapiro, B. Berche, and V. Mujica, J. Chem. Phys. **142**, 194308 (2015).
[36] M. Z. Hasan and C. L. Kane, Rev. Mod. Phys. **82**, 3045 (2010).
[37] X.-L. Qi and S.-C. Zhang, Rev. Mod. Phys. **83**, 1057 (2011).
[38] Z. F. Wang, Z. Liu, and F. Liu, Nat. Commun. **4**, 1471 (2013).
[39] Z. F. Wang, Z. Liu, and F. Liu, Phys. Rev. Lett. **110**, 196801 (2013).
[40] Z. F. Wang, N. Su, and F. Liu, Nano Lett. **13**, 2842 (2013).
[41] S. Ryu, A. P. Schnyder, A. Furusaki, and A. W. W. Ludwig, New J. Phys. **12**, 065010 (2010).
[42] M. Atala, M. Aidelsburger, J. T. Barreiro, D. Abanin, T. Kitagawa, E. Demler, and I. Bloch, Nat. Phys. **9**, 795 (2013).
[43] J. K. Asboth, B. Tarasinski, and P. Delplace, Phys. Rev. B **90**, 125143 (2014).
[44] Y. E. Kraus, Y. Lahini, Z. Ringel, M. Verbin, and O. Zilberberg, Phys. Rev. Lett. **109**, 106402 (2012).
[45] L.-J. Lang, X. Cai, and S. Chen, Phys. Rev. Lett. **108**, 220401 (2012).
[46] M. Mancini, G. Pagano, G. Cappellini, L. Livi, M. Rider, J. Catani, C. Sias, P. Zoller, M. Inguscio, M. Dalmonte, and L. Fallani, Science **349**, 1510 (2015).
[47] B. K. Stuhl, H.-I. Lu, L. M. Aycock, D. Genkina, and I. B. Spielman, Science **349**, 1514 (2015).
[48] S. Cheon, T.-H. Kim, S.-H. Lee, and H. W. Yeom, Science **350**, 182 (2015).
[49] The examples of celebrated single-helical molecules include single-stranded DNA and α-helical protein, where each nucleobase (amino acid) of single-stranded DNA (α-helical protein) is regarded as a single site.
[50] Y. A. Berlin, A. L. Burin, and M. A. Ratner, Chem. Phys. **275**, 61 (2002).
[51] C.-T. Shih, S. Roche, and R. A. Römer, Phys. Rev. Lett. **100**, 018105 (2008).
[52] T.-R. Pan, A.-M. Guo, and Q.-F. Sun, Phys. Rev. B **92**, 115418 (2015).
[53] A.-M. Guo and Q.-F. Sun, Phys. Rev. B **86**, 035424 (2012).
[54] P. G. Harper, Proc. Phys. Soc. London, Sect. A **68**, 874 (1955).
[55] D. R. Hofstadter, Phys. Rev. B **14**, 2239 (1976).
[56] The edge states are localized in either end of the helical molecules and are of zero dimension. Here, the edge denotes the two ends of the helical molecules.
[57] D. J. Thouless, M. Kohmoto, M. P. Nightingale, and M. den Nijs, Phys. Rev. Lett. **49**, 405 (1982).
[58] T. Fukui, Y. Hatsugai, and H. Suzuki, J. Phys. Soc. Jpn. **74**, 1674 (2005).
[59] A. P. Schnyder, S. Ryu, A. Furusaki, and A. W. W. Ludwig, Phys. Rev. B **78**, 195125 (2008).
[60] A. Kitaev, AIP Conf. Proc. **1134**, 22 (2009).
[61] N. S. Hush and A. S. Cheung, Chem. Phys. Lett. **34**, 11 (1975).
[62] Y. J. Yan and H. Zhang, J. Theor. Comput. Chem. **1**, 225 (2002).
[63] K. Senthilkumar, F. C. Grozema, C. F. Guerra, F. M. Bickelhaupt, F. D. Lewis, Y. A. Berlin, M. A. Ratner, and L. D. A. Siebbeles, J. Am. Chem. Soc. **127**, 14894 (2005).
[64] L. G. D. Hawke, G. Kalosakas, and C. Simserides, Eur. Phys. J. E **32**, 291 (2010).